Fibrosis-Related Gene and Protein Expression in Normal and Glaucomatous Trabecular Meshwork Cells

Yong-Feng Yang,[1] Paul Holden,[1] Ying Ying Sun,[1] Jennifer A. Faralli,[2] Donna M. Peters,[2,3] and Kate E. Keller[1]

[1]Casey Eye Institute, Oregon Health & Science University, Portland, Oregon, United States
[2]Departments of Pathology & Laboratory Medicine, University of Wisconsin, Madison, Wisconsin, United States
[3]Ophthalmology and Visual Sciences, University of Wisconsin, Madison, Wisconsin, United States

Correspondence: Kate E. Keller, Casey Eye Institute, Oregon Health and Science University, 3181 SW Sam Jackson Park Rd., Portland, OR 97239, USA; gregorka@ohsu.edu.

Received: December 19, 2024
Accepted: February 24, 2025
Published: March 24, 2025

Citation: Yang YF, Holden P, Sun YY, Faralli JA, Peters DM, Keller KE. Fibrosis-related gene and protein expression in normal and glaucomatous trabecular meshwork cells. *Invest Ophthalmol Vis Sci.* 2025;66(3):48. https://doi.org/10.1167/iovs.66.3.48

Purpose. Glaucomatous trabecular meshwork (GTM) tissue is characterized by excess fibrotic-like extracellular matrices, which negatively impacts aqueous humor outflow. Endothelial-to-mesenchymal transition (EndMT) is the process by which tissues develop fibrosis. In this study, we investigated fibrotic-related gene and protein profiles of non-glaucomatous trabecular meshwork (NTM) and GTM cells.

Methods. Primary cells were cultured from NTM ($n = 6$) and GTM ($n = 5$) age-matched cadaver eyes. RNA was harvested and mRNA profiling of 750 genes was performed using the human fibrosis panel (NanoString). Quantitative PCR (qPCR), Western blotting, and immunofluorescence microscopy were performed. A matrix metalloproteinase (MMP) fluorogenic assay was used to quantitate enzyme activity.

Results. Classic EndMT biomarkers, α-SMA, *SNAI2*, *TWIST1*, *TWIST2*, and *VIM*, were upregulated in GTM cells, whereas increased phosphorylated SMAD2-3 indicated increased TGFβ signaling. GTM cells had increased deposition of FN-EDA fibronectin fibrils, but reduced amounts of FN-EDB fibrils, and altered immunostaining of active $\alpha5\beta1$ and $\alpha v\beta3$ integrins. NanoString analysis showed that 2 genes were upregulated and 28 genes were downregulated in GTM cells compared with NTM cells. Western immunoblotting confirmed increased protein levels of N-cadherin and decreased MMP2, CHI3L1, COL6A3, and SERPINF1 proteins in GTM cells. Whereas MMP2 gene and protein levels were reduced, there was increased MMP activity.

Conclusions. Increased expression of α-SMA, FN-EDA, N-cadherin, *SNAI2*, *TWISTs*, *VIM*, TGFβ signaling, and MMP activity are consistent with GTM cells acquiring an EndMT phenotype. In combination with tissue studies, cultured GTM cells are a useful in vitro model for studying the fibrotic process in glaucoma.

Keywords: trabecular meshwork (TM), glaucoma, gene expression, fibrosis

The trabecular meshwork (TM) is the tissue that regulates aqueous humor outflow in the anterior eye and establishes intraocular pressure (IOP).[1] TM cells are tightly regulated at the molecular level to ensure that IOP is kept within a narrow range. In normal tissue, changes in the biomechanical environment caused by a sustained IOP elevation are detected by TM cells, which respond by initiating remodeling of the extracellular matrix (ECM) via increased activation of matrix metalloproteinase (MMP) enzymes. This facilitates fluid outflow to Schlemm's canal, which helps IOP to be lowered back to normotensive pressures.[2–5] TM dysfunction leads to elevated IOP, which can result in glaucoma, a major cause of blindness. Glaucomatous TM tissue is morphologically altered compared to normal age-matched tissue[6–12] and has fewer TM cells,[13] possibly due to increased cellular senescence.[14] Thus, cell loss in glaucomatous TM suggests that IOP elevations may not be efficiently detected and ECM remodeling responses are compromised compared with healthy individuals.

Fibrosis is a pathological process characterized by an accumulation of ECM in tissues leading to their dysfunction. It typically is initiated following an injury and follows a sequential series of events: inflammation, proliferation of pro-fibrotic cells, and ECM modifications resulting in accumulation of fibrous ECM, and stiffened tissues. In epithelial cells, a well-defined epithelial-to-mesenchymal transition (EMT) process is involved in fibrosis.[15,16] Endothelial cells undergo a similar process, which is known as endothelial-to-mesenchymal transition (EndMT). Both EMT and EndMT involve a series of molecular events that change their cellular phenotype to become more fibroblastic.[17–19] In EndMT, these changes include some combination of a downregulation of endothelial markers (e.g. VE-cadherin [CDH5], endothelial nitric oxide synthase [eNOS and NOS3], and CD31 [PECAM-1]) and increased expression of mesenchymal markers (e.g. SNAI, SLUG, SMAD3, αSMA, N-cadherin, and fibronectin).[20] Transforming growth factor-β (TGFβ) is a potent inducer of EndMT.[20] Of the three TGFβ family

members, TGFβ2 is the strongest inducer of EndMT[21] and it is elevated in the aqueous humor of patients with glaucoma.[22]

Numerous studies have sought to identify molecular differences between healthy and glaucomatous outflow pathway tissues.[1,23] Microarray studies comparing glaucomatous and non-glaucomatous age-matched tissue identified 72 upregulated genes and 84 downregulated genes, many of which were related to inflammation.[24] Another microarray study reported that 60 genes were differentially expressed, including 19 glycogenes, in POAG versus non-diseased TM tissue.[25] A larger study used Illumina gene expression chips to compare TM tissue from 15 patients with POAG and 13 healthy controls, which identified 480 differentially expressed genes including several ECM genes such as matrix Gla protein, SPARC, and TIMP2.[26] Proteomic studies identified cochlin as a protein that is enriched in glaucomatous TM tissue.[27] A chip-based study containing 60 biomarkers was performed on TM tissue from glaucoma ($n = 40$) and healthy subjects ($n = 20$) and found differential levels of several MMPs, cytokines (e.g. interleukins −10 and −6), chemokines (e.g. VCAM1), and growth factors (e.g. TGFβ1 and VEGF).[28] Electron microscopy analyses show the accumulation of plaque-like material surrounding elastic fibers as well as an abundance of lattice collagen.[8,9,29,30] In addition, numerous immunohistochemical studies demonstrated changes in ECM molecules in glaucomatous TM such as increased collagen types IV and VI in plaque-like material,[29,31] altered microfibrils composed of elastin and fibrillin-1,[32] decreased glycosaminoglycan sugar chain content,[33] altered thrombospondin-1,[34] and increased myocilin.[35] Excessive ECM accumulation in glaucomatous TM results in a stiffer tissue.[36–38] Together, these gene expression and protein studies support that glaucomatous TM tissue is molecularly different than non-glaucomatous, age-matched TM tissue, and that many of these changes are related to fibrosis.[39]

To better understand EndMT, fibrosis, and glaucoma, the purpose of this study was to investigate fibrosis-related mRNA and protein profiles of cultured non-glaucomatous and glaucomatous TM cells. Our study confirms that TM cells isolated from glaucomatous tissues demonstrate many of the changes in gene expression associated with EndoMT including elevated Fn-EDA and N-cadherin expression. It also provides novel information regarding differential expression of specific fibrosis-related molecules that could be involved in increased outflow resistance in glaucoma.

Materials and Methods

Cell Culture

Primary TM cells were cultured from normal and glaucomatous TM tissue derived from human cadaver eyes following best practice guidelines.[40] Whole globes were obtained from the eye bank (VisionGift, Portland, OR, USA) within 24 to 48 hours of death. Donor demographics and causes of death are shown in Table 1. Use of human cadaver tissue follows the guidelines from the Declaration of Helsinki and human tissue experiments complied with the guidelines of the ARVO Best Practices for Using Human Eye Tissue in Research (November 2021). All TM cells were characterized by their ability to upregulate myocilin protein following exposure to dexamethasone, some of which have been previously published, and others are shown in Supplementary Figure S1.[41–43] For experimental assays, TM cells were cultured for 3 days in DMEM containing 2.5 g/L glucose +10% fetal calf serum (FCS) + 1% penicillin-streptomycin and, following a wash with PBS, they were placed in serum-free DMEM containing 0.1 mM ascorbate. This concentration mimics that of ascorbate levels in the aqueous humor.[44] After culturing for a further 3 days, the cells were harvested for RNA and protein. TM cells used for NanoString experiments were used at passage 4. TM cells for validation assays were used between passages 4 and 6.

RNA Isolation and Nanostring nCounter Sprint Profiler Analysis

RNA was harvested from confluent TM cells using the RNA Easy micro kit (Qiagen, Germantown, MD, USA). RNA concentrations were determined using the NanoDrop One and showed an average of 120 ng/µL (range = 80–150 ng/µL, $n = 12$). Each sample, containing a total of 100 ng RNA diluted in water to a volume of 5 µL, was mixed with 8 µL of hybridization master mix (5 µL hybridization buffer and 3 µL reporter probe human fibrosis v2.1 codesets) and 2 µL capture probe sets (NanoString Technologies, Seattle, WA, USA). The reporter codesets contain half of the target-specific sequence and six fluorescently labeled RNA segments (barcodes) of four different colors, whereas the capture probe sets contained a biotin label and the other half of the target-specific sequence. Samples were hybridized at 65°C for 18 hours in a thermocycler and then the hybridized samples were injected into nCounter Sprint cartridges and scanned with an nCounter SPRINT profiler instrument. One barcode count is equivalent to one RNA molecule. Raw data files (*.RCC) were generated for each sample and were uploaded to Rosalind informatics software (San Diego, CA, USA). Digital counts were pruned by the software to remove low expressing housekeeping genes prior to normalization, which aids data clarity, improves accuracy, and increases computational efficiency. Data were then normalized to the remaining 10 internal housekeeping genes on the panel. Genes in TM samples with low counts (<40), which were comparable to negative control counts, were removed and a total of 510 genes were analyzed. Differentially expressed genes were identified using a cutoff of ≥ 1.5 or ≤ -1.5 fold change and were considered significant if the P value was < 0.05. To investigate pathways, differentially expressed genes were uploaded to ShinyGO, version 0.8 (South Dakota State University, Brookings, SD, USA).

Quantitative PCR

To confirm NanoString results, we performed TaqMan quantitative RT-PCR (qRT-PCR) with predesigned primer-probe sets (ThermoFisher, Grand Island, NY, USA). The catalog numbers are listed in Supplementary Table S3. Briefly, 500 ng RNA was transcribed into cDNA using Superscript III reverse transcriptase (ThermoFisher). The cDNA was mixed with the primer-probes and TaqMan fast Advanced master mix and then DNA products were amplified on a QuantStudio 3 thermocycler (Applied Biosystems, Waltham, MA, USA) using the following amplification cycles: 95°C for 2 seconds, 45 cycles of 95°C for 1 second, and 60°C for 20 seconds. All data were normalized to 18S RNA, which was used as a housekeeping gene. Results were analyzed using a geometric mean to calculate $\Delta\Delta$Ct. Other genes were amplified

Investigative Ophthalmology & Visual Science

Table 1. Summary of Donor Eyes

Cell Strain	Age	Sex	Cause of Death	Glaucoma Status	Experiment Used	Ref. Myoc Induction
Normal TM Cells						
2022-0794	80	M	Respiratory failure with hypoxia	—	Nanostring, Western blot, qPCR	Supplementary Fig. S1
2022-0140	77	F	Cardiogenic shock	—	Nanostring, qPCR, MMP assay	
2021-1110	77	F	Lung cancer	—	Nanostring, qPCR, MMP assay, Western blot	[43]
2022-0791	59	M	Mantle cell lymphoma	—	Nanostring, IF, Western blot, qPCR	Supplementary Fig. S1
2021-1323	57	M	Cardiac arrest	—	Nanostring, qPCR, Western blot, MMP assay	[43]
2021-1493	74	F	Subdural bleed	—	Nanostring, qPCR, Western blot, MMP assay	Supplementary Fig. S1
2018-1233	53	M	Lung cancer	—	MMP assay, IF	[43]
2018-0070	54	M	Cardiac arrest	—	MMP assay, IF, Western blot	[43]
2021-1328	75	M	Cardiac arrest	—	MMP assay, Western blot	[43]
2020-0984	69	M	Advanced Parkinsons, dementia	—	MMP assay, IF, Western blot	[43]
2018-1341	55	M	Myocardial infarction	—	Western blot, IF	[43]
N81LM	81	M	Unknown	—	qPCR	In review
Glaucoma TM cells						
2018-1672	57	M	Respiratory failure	Glaucoma	Nanostring, IF Western blot, qPCR	[41]
2019-1757	92	F	Cardiogenic shock	POAG (Latanoprost)	Nanostring, IF Western blot, qPCR	[43]
2019-1150	81	F	Metastatic breast cancer	POAG (Combigan)	Nanostring, Western blot, qPCR	Supplementary Fig. S1
2022-1033	78	M	Cardiac arrest	Bilateral OAG	Nanostring, Western blot, qPCR	Supplementary Fig. 1
2022-0949	61	F	Pneumonia	POAG	Nanostring, qPCR	Supplementary Fig. 1
2018-0374	79	M	Ischemic cerebrovascular accident	Glaucoma (Timolol)	Western blot, IF	[41]
2019-0406	81	F	Septic shock	Open angle glaucoma	Western blot, IF	[43]
2020-1607	83	F	Myocardial infarction	POAG	Western blot, IF	Supplementary Fig. S1
2018-0524	83	M	Cardiac and respiratory arrest	Glaucoma	MMP assay	[41]
2020-0899	94	F	Acute diastolic heart failure	POAG	MMP assay	[43]
2021-1368	96	M	Cardiac arrest	Glaucoma (Latanoprost)	MMP assay, Western blot	Supplementary Fig. S1

IF, immunofluorescence.

using primers in Supplementary Table S3 (Integrated DNA Technologies, Coralville, IA, USA) and normalized to HPRT1 as a housekeeping gene, following a previously published method.[45]

Western Immunoblotting and Densitometry

After 3 days in ascorbate-containing media, cell lysates were harvested with RIPA buffer while serum-free conditioned media was collected from the cultures. Total protein in each RIPA lysate was measured using a Pierce BCA protein assay (ThermoScientific). Equal amounts of protein were loaded into each lane of the SDS-PAGE gels. RIPA lysates were mixed with SDS-PAGE loading buffer containing 0.1 mM dithiothreitol. Proteins in conditioned media were measured using a Bradford Plus protein assay kit (ThermoScientific) and equal amounts were precipitated using 20% (w/v) trichloroacetic acid and washed with ice-cold acetone, before the pellet was resuspended in 1x SDS-PAGE loading buffer containing 0.1 mM dithiothreitol. Proteins in each sample were separated by 10% SDS-PAGE (BioRad Laboratories, Hercules, CA, USA). Coomassie blue staining was performed on conditioned media from each sample. Reduced proteins were transferred to nitrocellulose membranes, blocked with blocking buffer (ThermoScientific, cat # 37572), and probed with one or more of the primary antibodies (Supplementary Table S4). Primary antibodies were detected with the appropriate species secondary antibody conjugated to either IRDye800 or IRDye700 (Rockland Immunochemicals, Gilbert, PA, USA). Immunoblots and Coomassie stained gels were imaged using

Investigative Ophthalmology & Visual Science

the Odyssey DLx imager (Licor) and pixel density of the bands in each lane was quantitated using ImageJ software. Background was subtracted from experimental relative fluorescent units (RFUs) data. Proteins in RIPA lysates were normalized to the loading controls stated in the figures. To normalize media gels, a box was drawn around the entire vertical lane of a Coomassie-stained gel (Supplementary Fig. S3). Each lane was assigned a correction factor compared to the first lane. Thus, the first lane had a correction factor of 1 and the other lanes had correction factors ranging from 0.8 to 1.1. The RFU value measured from the immunoblot was then multiplied by this correction factor to normalize for loading and each data point was plotted on a bar graph.

MMP Assay

The SensoLyte 520 generic MMP assay kit (Anaspec, Inc., Fremont, CA, USA) were performed as described previously.[46,47] Briefly, confluent non-glaucomatous trabecular meshwork (NTM) and glaucomatous trabecular meshwork (GTM) cells were grown to confluence, changed to serum-free media, and cultured for 3 days. Media and cell lysates were harvested, the MMPs were activated by incubating with 1 mM 4-aminophenylmercuric acetate for 90 minutes at 37°C, and then 5-fluorescein amidite (FAM)-labeled fluorescent substrate was added. This substrate contains a quencher, which is removed following MMP cleavage, and 5-FAM fluorescence was then measured on a plate reader (Ex/Em = 490/520 nm). Thus, the RFUs are directly correlated to MMP activity in each sample. RFUs were then normalized to total protein in each sample, as measured by a bicinchoninic acid (BCA) assay. Each sample was measured in duplicate and averaged. Data from individual NTM or GTM biological replicates were then plotted.

Immunohistochemistry and Immunofluorescence

TM tissue wedges, dissected approximately 180 degrees apart from one anterior segment, were fixed in 4% paraformaldehyde for 4 hours and then embedded into a single paraffin block. Five µm radial sections were cut approximately perpendicular to Schlemm's canal at the pathology/histology core facility of the Knight Cancer Institute (Oregon Health & Science University, Portland, OR, USA). Tissue sections were then deparaffinized, blocked with CAS-Block (ThermoFisher), and then incubated with the stated primary antibodies (see Supplementary Table S4) for 2 hours. Alexa-fluor 488- or 594-conjugated secondary antibodies (ThermoFisher) from the appropriate species were then incubated. After washing with PBS, coverslips were mounted in ProlongGold mounting medium containing DAPI (ThermoFisher). Tissue sections were visualized using a Fluoview FV1000 confocal microscope (Olympus) and the images were processed using FIJI software.

For immunofluorescence, NTM and GTM cells were seeded on collagen type I-coated silicone membranes of BioFlex 6-well culture plates (FlexCell International, Burlington, NC, USA) and cultured for 3 days, as we described previously.[43,48] After removing the silicone membranes (with attached cells) from the plate, the cells were fixed with 4% paraformaldehyde, permeabilized with 0.1% Triton X-100, and incubated with primary antibodies (see Supplementary Table S4) diluted 1:50 in phosphate-buffered saline (PBS). After washing, the cells were labeled with an Alex Fluor 488-conjugated donkey anti-mouse, or Alex Fluor 594-conjugated donkey anti-rabbit antibodies. After washing, glass coverslips were mounted with ProLong gold antifade containing DAPI (Invitrogen) to stain DNA in nuclei. The focal adhesion areas were measured with FIJI software using a published protocol.[49]

Statistics

Data were plotted using box and whisker graphs (box extends from 25–75th percentile, the line is the median, and the whiskers indicate the minimum and maximum values), or bar charts (mean ± SEM). Individual data points are overlaid onto the graphs, and "n" are stated in the figure legends. Data were statistically analyzed using an unpaired *t*-test in Graphpad Prism 10 (Boston, MA, USA). Any P value < 0.05 was considered significant.

Results

Primary TM cells were cultured from non-glaucomatous ($n = 6$) and glaucomatous ($n = 5$) cadaver eyes. The donors were age- and sex-matched (NTM: mean age = 70.6 ± 4 years, range = 57–80, 3 male donors and 3 female donors; GTM: mean age = 73.8 ± 5.9 years, range = 57–92, 2 male donors and 3 female donors; see Table 1). All donors were Caucasian. Prior studies showed that cellular senescence of our GTM cell cultures was similar to that of NTM cells.[41] In addition, qPCR of the senescence biomarkers, *CBX7* and *p21cip*, show no significant expression differences between NTM and GTM cells (Supplementary Fig. S2).

GTM cells are known to show increased expression of alpha-smooth muscle actin (α-SMA) and fibronectin.[50,51] Because α-SMA, fibronectin, and TGFβ are upregulated in EndMT,[17] we performed Western immunoblotting to assess their expression levels in cultured NTM and GTM cells. Densitometry showed a significant increase in α-SMA ($P = 0.005$) protein levels in GTM cell lysates (Fig. 1A). To assess TGFβ signaling, we assessed phosphorylation of SMAD2-3 protein, which is an intracellular protein downstream from the TGFβ receptor. After normalizing to total SMAD2, there was significantly increased phosphorylated SMAD2-3 in GTM cells (Fig. 1B, $P = 0.016$). The qRT-PCR (Fig. 1C), or Western immunoblotting of conditioned media (Fig. 1D) showed that fibronectin levels were significantly increased in GTM cells. Fibronectin mRNA is alternatively spliced and the resulting protein isoforms can include extra domain A (FN-EDA) and/or extra domains B (FN-EDB).[51] Because FN-EDA is increased in glaucomatous tissue,[52] we also investigated EDA and EDB transcripts in NTM and GTM cells (see Fig. 1C). FN-EDA was significantly increased ($P = 0.0007$), whereas FN-EDB was decreased, although not significantly ($P = 0.19$).

In addition, we investigated fibronectin and its isoforms by immunofluorescence (Fig. 2). When using an antibody that detects total fibronectin, there was increased fibronectin fibrils in GTM cells when normalized to the number of nuclei in a field (see Figs. 2A, 2C, $P = 0.007$). EDA and EDB were detected using specific monoclonal antibodies. When normalized to nuclei, there was a significant increase for EDA-containing fibronectin fibrils (see Figs. 2A, 2C, $P = 0.008$), but FN-EDB fibrils were significantly decreased (see Figs. 2B, 2C, $P = 0.007$). Thus, whereas the fibronectin protein levels are increased, the proportion of FN-EDB fibrils are reduced in GTM cells.

Investigative Ophthalmology & Visual Science

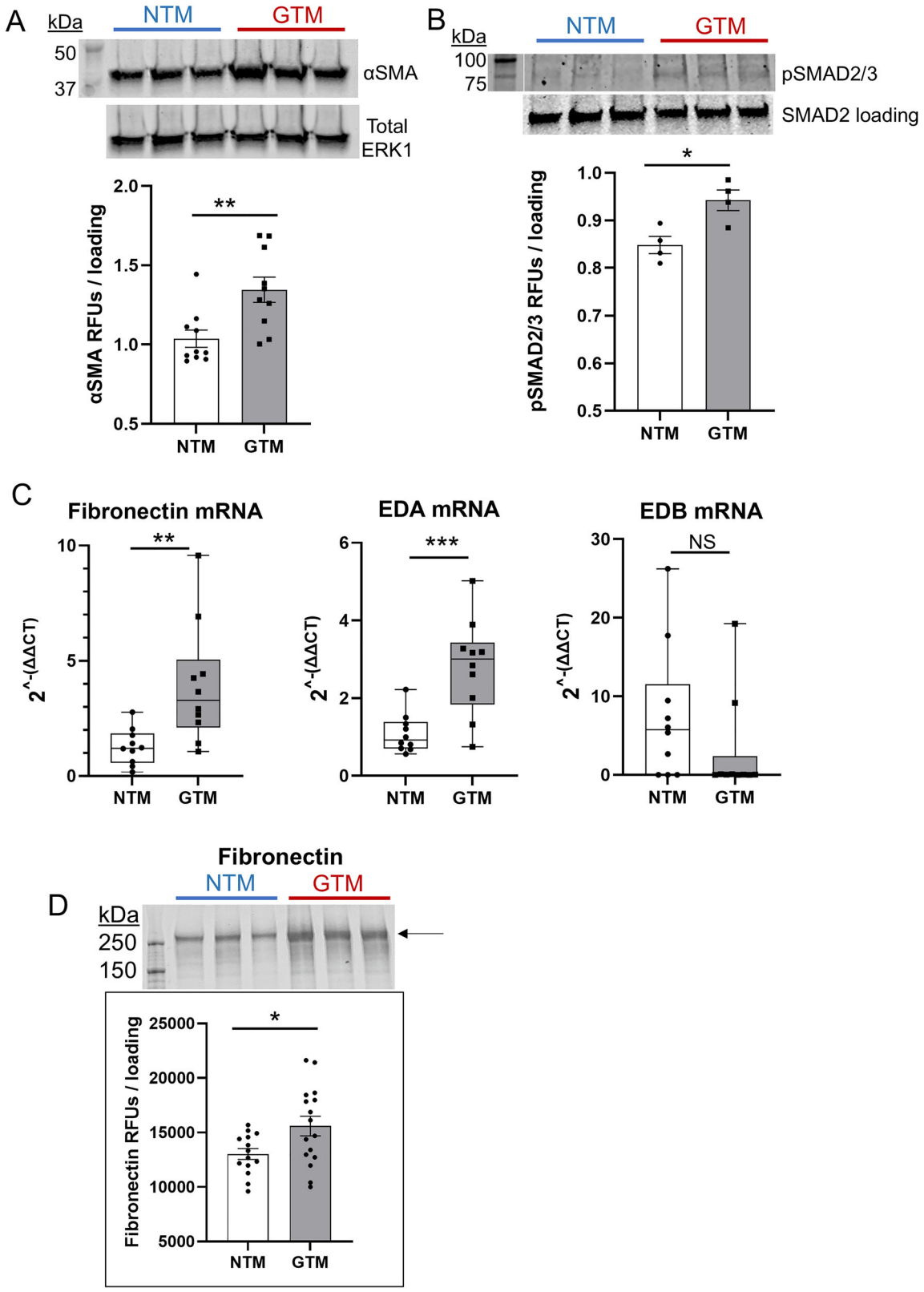

Figure 1. Gene expression and protein levels in glaucoma (GTM) versus non-glaucomatous (NTM) trabecular meshwork cells. (**A**) Representative Western immunoblot showing upregulation of alpha-smooth muscle actin (αSMA) in glaucoma TM cell lysates compared with NTM cells ($n = 3$ biological replicates). Loading control was total ERK. Densitometry quantifying αSMA relative fluorescent units (RFUs) ± SEM normalized for the loading. $^{**}P = 0.005$; $n = 10$ each group from 9 (NTM) or 8 (GTM) biological replicates. (**B**) Western blots and densitometry of phosphorylated SMAD2/3 levels in GTM and NTM cell lysates, with total SMAD2 as loading control. Densitometry quantifying phosphoSMAD2/3 RFUs ± SEM normalized for total SMAD2. $^{*}P = 0.016$; $n = 4$ each group from 4 biological replicates. (**C**) Quantitative RT-PCR of total fibronectin, as well as the EDA and EDB isoforms of fibronectin ($^{**}P = 0.006$; $^{***}P = 0.0007$; $n = 10$ biological replicates; NS = not significant). (**D**) Representative Western immunoblot and densitometry of fibronectin protein RFUs ± SEM in conditioned media showed significant increases in GTM cells. $^{*}P < 0.05$; $n = 14$ for NTM from 7 biological replicates; $n = 16$ for GTM from 6 biological replicates.

Investigative Ophthalmology & Visual Science

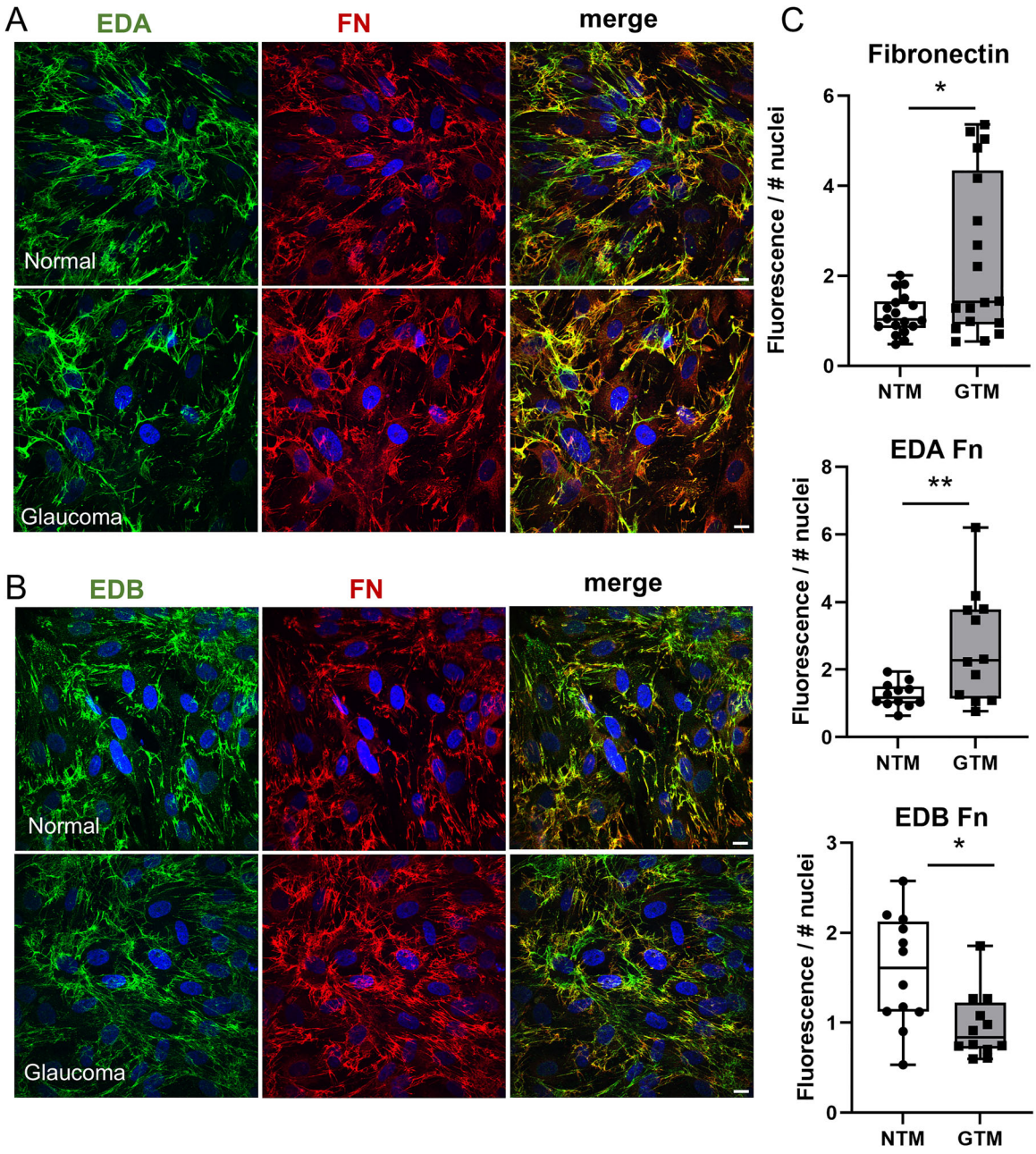

Figure 2. Immunofluorescence of fibronectin and its isoforms, EDA and EDB. Immunofluorescence of NTM and GTM cells stained with (**A**) EDA (IST9 monoclonal; *green*) or (**B**) EDB (BC1 monoclonal; *green*) and pan-fibronectin (rabbit polyclonal; *red*). *Scale bar* = 20 µm. (**C**) Total fluorescence signal in each confocal image was measured using ImageJ and normalized to the number of nuclei in a field. Total fibronectin, $*P = 0.007$, $n = 18$ images from 3 biological replicates; EDA ($**P = 0.008$) and EDB ($*P = 0.007$) from $n = 12$ images from 4 biological replicates.

We also investigated immunostaining of $\alpha5\beta1$ integrin, the fibronectin receptor. A monoclonal antibody, which recognizes the active form of $\alpha5\beta1$,[53] immunolabeled fibrillar adhesions in two biological replicates of NTM (Fig. 3A). In GTM cells, the pattern was much more punctate. We also assessed $\alpha v\beta3$ integrin because activation of $\alpha v\beta3$ integrin is considered to be pro-fibrotic in TM cells.[54] In NTM cells, $\alpha v\beta3$ integrin was localized to focal adhesions as expected (Fig. 3B). In GTM cells, active $\alpha v\beta3$ integrin immunostaining in focal adhesions was more extensive. Focal adhesion areas were significantly increased in GTM cells. Together, these results demonstrate that our cultured GTM cells upregulate several proteins that were previously reported to be associated with glaucoma.[24,52]

The purpose of this study was to investigate fibrosis-related profiles of GTM cells, so we chose to use a NanoString panel, rather than RNAseq, to focus on fibrosis genes. RNA isolated from NTM and GTM cells was analyzed for differentially expressed genes (DEGs) using fluorescent barcode technology. Of 760 endogenous genes on the panel (Supplementary Table S1), 510 genes gave a fluo-

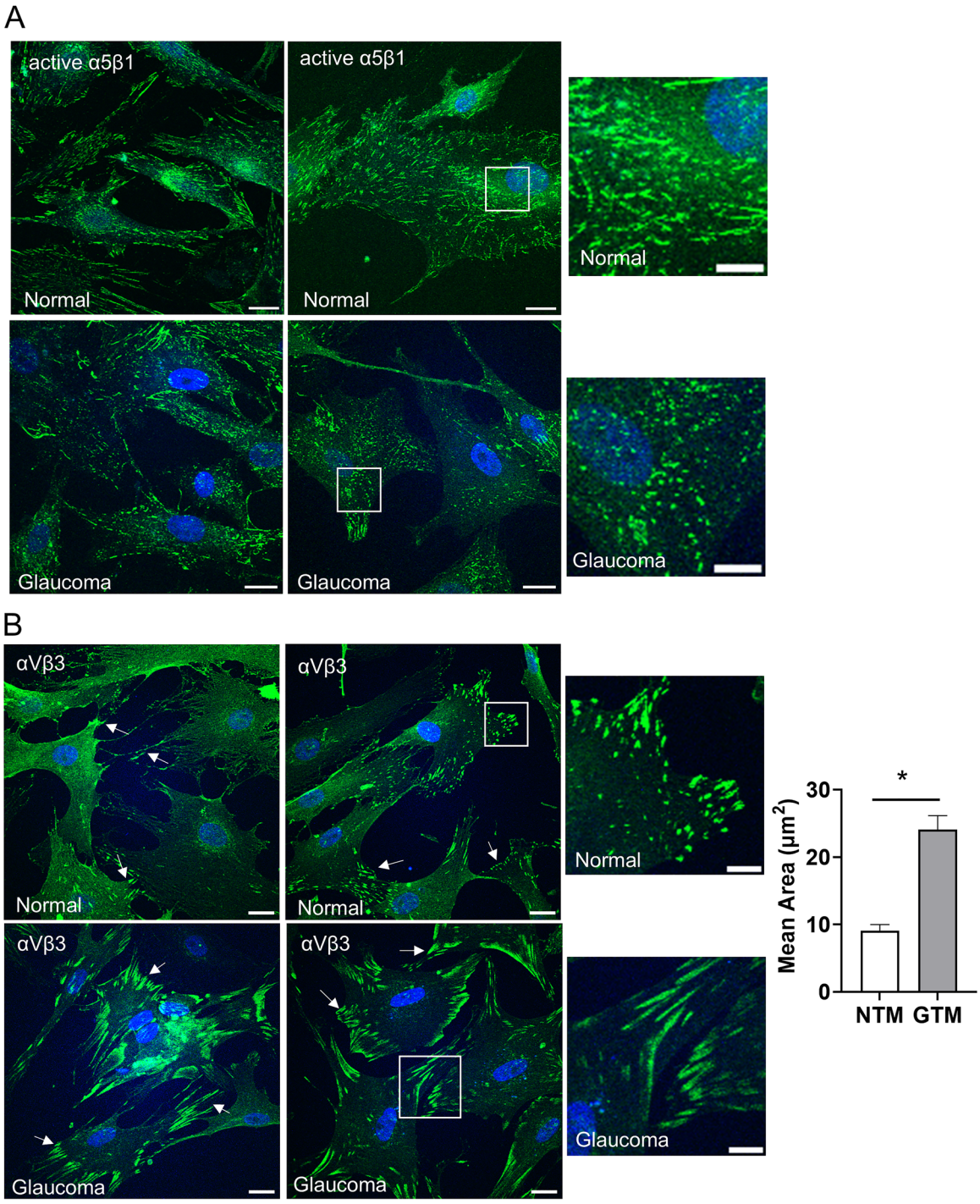

Figure 3. Integrins $\alpha5\beta1$ and $\alpha v\beta3$ in NTM and GTM cells. Immunofluorescence of two representative NTM and GTM cell strains immunostained with an antibody that detects (**A**) active $\alpha5\beta1$ integrin or (**B**) total $\alpha v\beta3$ integrin. *Boxed areas* are shown at higher magnification. *Arrows* point to $\alpha v\beta3$ integrin in focal adhesions. *Scale bar* = 20 µm; insets, *scale bar* = 10 µm. The areas of $\alpha V\beta3$-stained focal adhesions were measured from three biological replicates of NTM and GTM, as described in the Methods section. *$P < 0.0001$.

rescent signal above background values (Supplementary Table S2). Of these 510 genes, 30 genes were differentially expressed. Two genes were significantly upregulated, and 28 genes were significantly downregulated in glaucomatous TM cells versus non-glaucomatous cells (Table 2). A heatmap of the clustering of the NTM and GTM samples is included as Supplementary Figure S4. A volcano plot showing the up (red) and downregulated (blue) genes is shown (Fig. 4A). To validate the NanoString results, TaqMan qPCR was used. The results showed that *VCAM1*, *IL33*, and *F11R* (also known as *JAM1*) were significantly downregulated (Fig. 4B), whereas *VEGFA* and *POSTN* were up and downregulated, respectively, but these did not reach significance ($P = 0.345$ and $P = 0.101$, respectively). The 30 significantly

Investigative Ophthalmology & Visual Science

Table 2. Differentially Expressed Genes in Glaucoma ($n = 5$) Versus Normal ($n = 6$) TM Cells (FC > 1.5 or < 1.5; $P < 0.05$)

Name	Description	FC	Log FC	*P* Value
Upregulated				
VEGFA	Vascular endothelial growth factor A	1.677	0.746	0.001
CDH2	Cadherin 2, type 1, N-cadherin (neuronal)	1.611	0.688	0.043
Downregulated				
IL6ST	Interleukin 6 signal transducer	−1.514	−0.599	0.025
TLR1	Toll-like receptor 1	−1.624	−0.700	0.018
S100A4	S100 calcium binding protein A4	−1.625	−0.700	0.041
BCL2	B-cell CLL/lymphoma 2	−1.631	−0.706	0.015
CASP7	Caspase 7, apoptosis-related cysteine peptidase	−1.636	−0.710	0.009
HVCN1	Hydrogen voltage gated channel 1	−1.716	−0.779	0.005
PLTP	Phospholipid transfer protein	−1.750	−0.807	0.002
CDON	Cell adhesion associated, oncogene regulated	−1.751	−0.808	0.047
ISG20	Interferon stimulated exonuclease gene 20 kDa	−1.776	−0.829	0.001
CXCL12	Chemokine (C-X-C motif) ligand 12	−1.785	−0.836	0.020
SMAD6	SMAD family member 6	−1.802	−0.850	0.003
ACVRL1	Activin A receptor type II-like 1; ALK1	−1.811	−0.857	0.018
ELN	Elastin	−1.946	−0.960	0.041
MMP2	Matrix metallopeptidase 2	−2.146	−1.101	0.015
IFI27	Interferon, alpha-inducible protein 27	−2.319	−1.213	0.044
COL6A3	Collagen, type VI, alpha 3	−2.388	−1.256	0.043
SERPING1	Serpin peptidase inhibitor, clade G (C1 inhibitor), member 1	−2.436	−1.284	0.012
F11R	F11 receptor	−2.464	−1.301	0.018
SERPINF1	Serpin peptidase inhibitor, clade F (alpha-2 antiplasmin, pigment epithelium derived factor), member 1	−2.758	−1.464	0.009
IL1R1	Interleukin 1 receptor, type I	−2.832	−1.502	0.000
CD14	CD14 molecule	−3.309	−1.726	0.001
VCAM1	Vascular cell adhesion molecule 1	−3.481	−1.800	0.000
HSD11B1	Hydroxysteroid (11−beta) dehydrogenase 1	−4.142	−2.050	0.000
IL11	Interleukin 11	−4.283	−2.099	0.008
POSTN	Periostin, osteoblast specific factor	−4.393	−2.135	0.019
TNFSF10	Tumor necrosis factor (ligand) superfamily, member 10	−4.516	−2.175	0.016
CHI3L1	Chitinase 3-like 1 (cartilage glycoprotein-39)	−6.115	−2.612	0.008
IL33	Interleukin 33	−8.611	−3.106	0.001

CLL, chronic lymphatic leukemia.

DEGs were analyzed with ShinyGO tool for gene enrichment analysis (Fig. 4C). The top 10 GO:Molecular function and GO:Biological process pathways identified pathways such as regulation of response to stimuli, signal transduction, cellular communication, and stress, as well as signal receptor binding and activity, cytokine activity, cell adhesion, and growth factor receptor binding. The top five identified Kyoto Encyclopedia of Genes and Genomes (KEGG) pathways included cytokine receptor interaction, NF-κB signaling, and fluid shear stress. As the majority of the DEGs were downregulated, these pathways would be negatively impacted.

We then chose several DEGs to further investigate based on their function in EndMT. *CDH2* is expressed in TM cells and is upregulated by TGFβ.[55] As shown in Figure 5, N-cadherin mRNA expression and protein levels were significantly increased in GTM cells compared with age-matched NTM cells. Densitometry showed an approximately 26.7% increase in N-cadherin protein in GTM cells (see Fig. 5B). These data agree with the NanoString data. Immunofluorescence of NTM and GTM cells also showed an increased N-cadherin fluorescent signal in GTM cells (see Fig. 5C), whereas N-cadherin was detected in the TM of normal and glaucomatous tissue sections (see Fig. 5D). Positive immunostaining was observed in the TM cells on the TM beams, as well as in juxtacanalicular (JCT) region and inner wall (IW) of Schlemm's canal.

Matrix metalloproteinase-2 (MMP2) is potent enzyme that has a major role in ECM remodeling in the TM.[4] It degrades many extracellular components including collagens, elastin, proteoglycans, thrombospondin, and fibronectin.[5] Consistent with the NanoString gene expression data, MMP2 protein levels were significantly decreased in GTM cells (Fig. 6A, $P = 0.016$). Although the MMP2 protein levels in NTM cells were consistent across the four cell strains, there was some variability in MMP2 levels in GTM cells. We also assessed MMP activity in conditioned serum-free media and cell lysates. Please note that this assay is not MMP2 specific, rather the fluorogenic peptide can be cleaved by multiple MMPs. Whereas the increases in MMP activity in the conditioned media of GTM cells were significant ($P = 0.047$), those in the cell lysates were not ($P = 0.068$; Fig. 6B). We also investigated MMP2 localization in NTM and GTM cells by immunofluorescence (Fig. 6C). In NTM cells, MMP2 was located to podosome or invadopodia-like structures (PILS), areas of focal ECM degradation.[48] These showed typical ring-like, circular patterns of immunostaining. However, in GTM cells, the MMP2 labeling was more extensive and, while the rings were still apparent, in some cases, they appeared to cluster into larger structures.

Investigative Ophthalmology & Visual Science

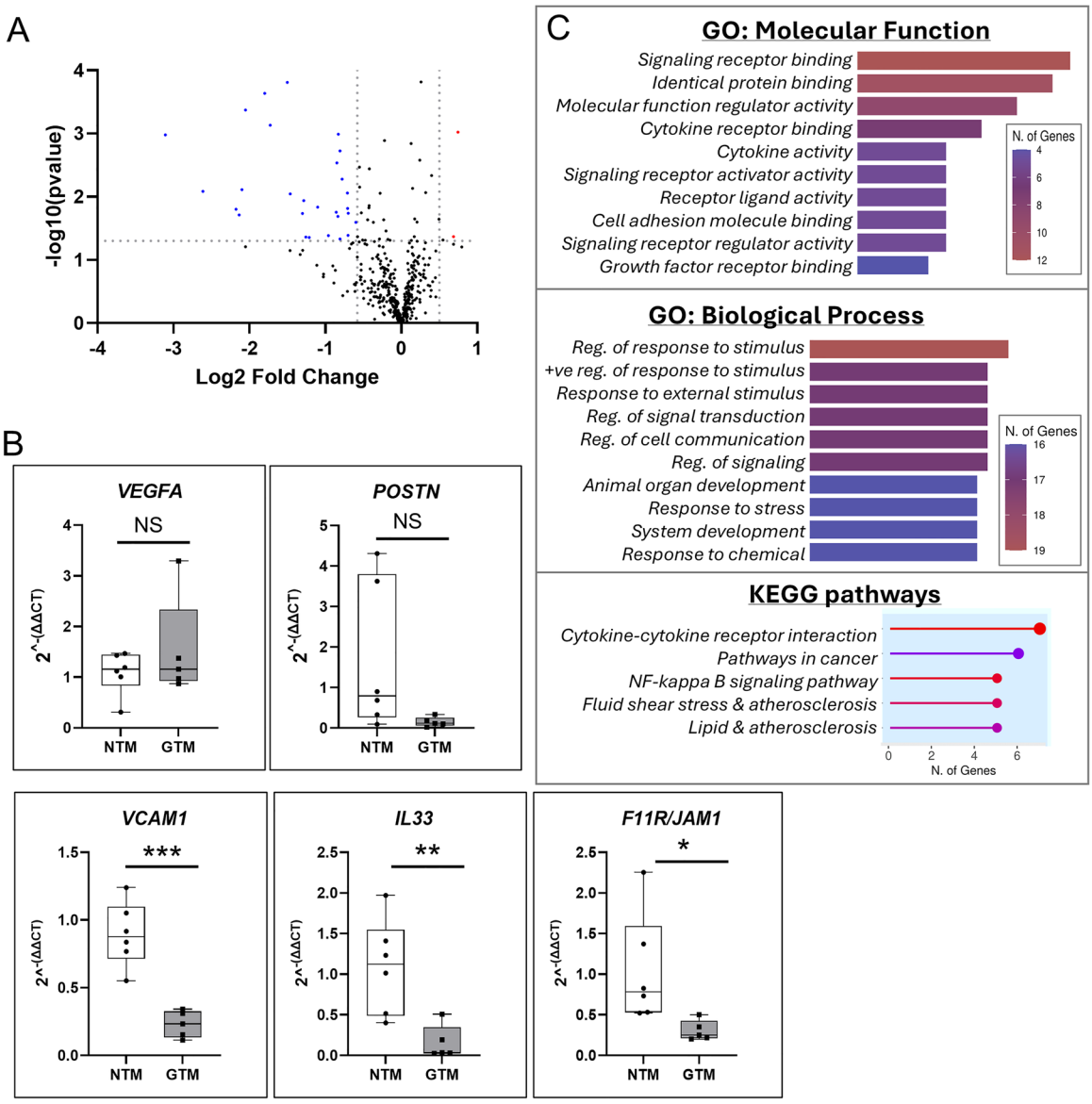

Figure 4. Quantification of fibrosis-related genes in NTM and GTM cells using NanoString barcode technology. (**A**) A volcano plot shows all 510 genes on the cartridge that produced a fluorescent signal. Significantly upregulated genes are shown in *red* and downregulated genes are shown in *blue*. (**B**) Quantitative RT-PCR using Taq Man primer-probes of selected up (*VEGF*) and downregulated (*POSTN*, *F11R/JAM1*, *VCAM1*, and *IL33*) genes. NTM, $n = 6$ biological replicates; GTM, $n = 5$ biological replicates; *$P < 0.05$; **$P < 0.01$; ***$P < 0.001$; NS = not significant. (**C**) Top 10 GO: molecular function, top 10 GO: biological process and top 5 KEGG pathways for the 30 significant DEGs, as determined by ShinyGO version 0.8 analysis. As the majority of genes are downregulated, these pathways would be negatively impacted.

Three additional DEGs we chose to investigate were *CHI3L1*, *COL6A3*, and *SERPINF1*, which was based on their regulation or dysregulation in the glaucomatous outflow pathway. Chitinase-3-like-1 (CHI3L1) is a 40 kDa secreted glycoprotein that is strongly expressed in TM and is often used as a biomarker of TM cells.[56] By qPCR, *CHI3L1* mRNA expression was significantly decreased (Fig. 7A, $P < 0.01$) and similarly, there was a significant 45% decrease in CHI3L1 protein levels in GTM cells (Fig. 7B, $P = 0.02$). However, there was considerable variability in protein levels with some cell strains showing robust levels, whereas others had little to no CHI3L1 protein. In GTM tissue, the CHI3L1 distribution appeared to be disrupted compared to age-matched NTM tissue (Fig. 7C). In healthy tissue, CHI3L1 is distributed in the innermost TM, but is not abundant in the JCT region. Conversely, CHI3L1 in glaucomatous tissue is patchier and shows high levels in the JCT region. *COL6A3* gene variants have been associated with glaucoma and COL6A3 protein levels were significantly reduced in GTM cell cultures by immunofluorescence.[57,58] In this current study, qPCR data and Western immunoblotting analyses show that *COL6A3* mRNA expression and protein levels were significantly reduced in GTM cells (Figs. 8A, 8B). Please note that COL6A3 has multiple bands due to alternative splicing and procollagen processing. *SERPINF1*, also known as pigment epithelium derived factor (PEDF), is a 50 kDa secreted serine protease inhibitor that is a component of aqueous humor and its levels are decreased with age and glaucoma.[59] In our

Investigative Ophthalmology & Visual Science

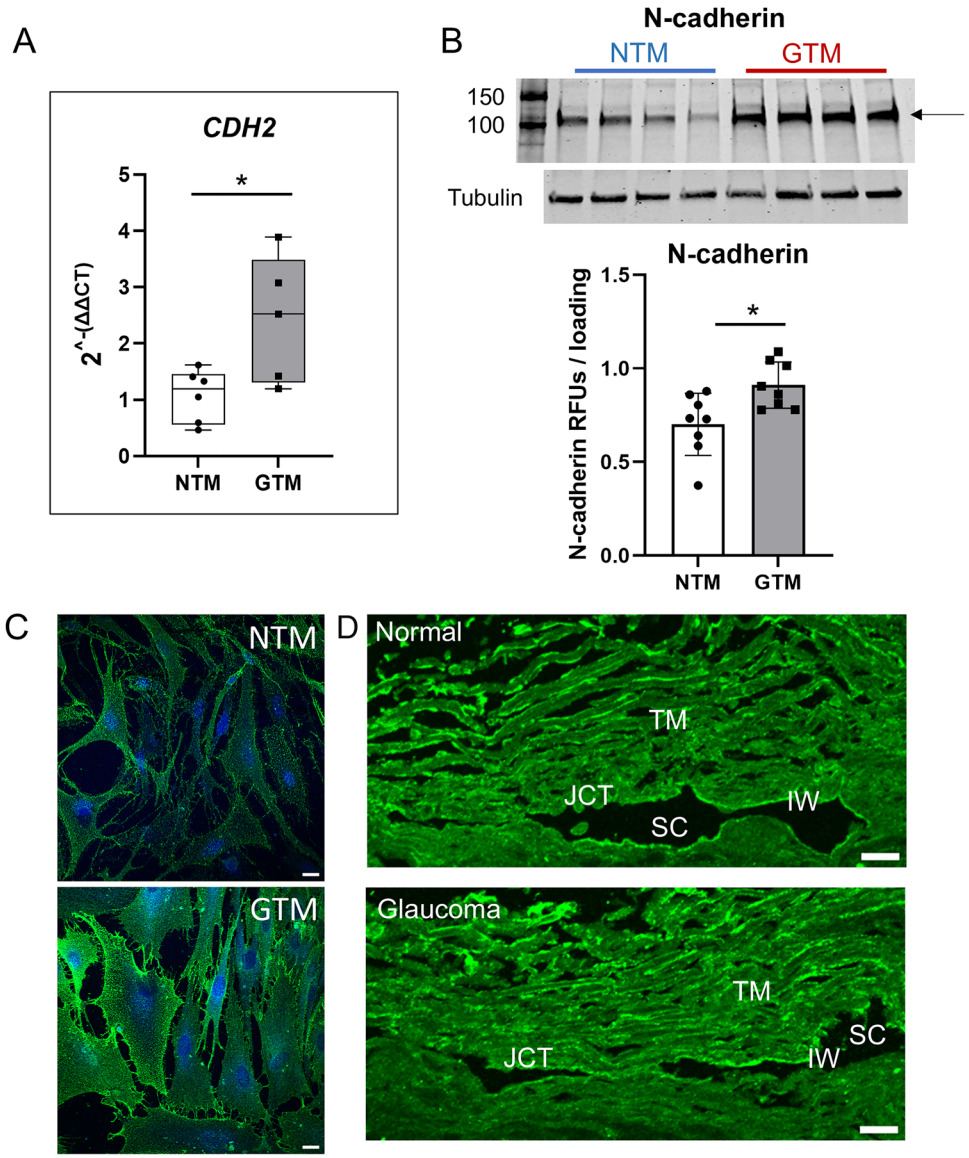

Figure 5. N-cadherin (*CDH2*) in NTM and GTM cells. (**A**) Quantitative RT-PCR using Taq Man primer-probes shows significant upregulation of the *CDH2* gene in GTM cells. NTM, $n = 6$ biological replicates; GTM, $n = 5$ biological replicates; $^*P < 0.05$. (**B**) Western immunoblot and densitometry of N-cadherin protein RFUs ± SEM in cell lysates showed a significant increase in N-cadherin in GTM cells. Tubulin is the loading control. $^*P = 0.012$; $n = 8$ from 4 biological replicates. (**C**) Representative immunofluorescence images of N-cadherin in NTM and GTM cells showing increased N-cadherin immunostaining in GTM cells. Scale bar = 20 µm. (**D**) N-cadherin distribution in healthy and glaucoma TM tissue. IW, inner wall of Schlemm's canal; JCT, juxtacanalicular region; SC, Schlemm's canal; TM, trabecular meshwork. *Scale bar* = 20 µm.

study, *SERPINF1* mRNA was significantly reduced by qPCR in GTM cells, but although PEDF protein levels were decreased (approximately 23%), this did not reach significance (Figs. 8C, 8D, $P = 0.106$).

Finally, we quantified expression of several of the EndMT mesenchymal biomarkers described for vascular endothelial cells, including *SNAI1*, *SNAI2* (SLUG), *TWIST1*, *TWIST2*, *VIM* (vimentin), and *S100A4*. RT-PCR analysis using mRNA from the same cell strains used for the NanoString analysis as well as additional biological replicates, showed significant upregulation of the mesenchymal biomarkers *SNAI2*, *TWIST1*, *TWIST2*, and *VIM* in GTM cells (Fig. 9). However, *S100A4* and *SNAI1* showed no significant difference in qPCR assays.

Discussion

EndMT is considered a key factor in the development of fibrotic-like changes to tissues and is characterized by the upregulation of mesenchymal markers and downregulation of endothelial markers.[17,20] Using TM cells isolated from age-matched healthy and glaucomatous tissues, our studies show that glaucomatous TM cells exhibit several critical DEGs associated with EndMT.

Among classical EndMT markers, we found a significant upregulation of αSMA, fibronectin, Fn-EDA, N-cadherin, *SNAI2*, *VIM*, *TWIST1*, and *TWIST2*. Furthermore, GTM cells exhibited elevated levels of SMAD2/3 phosphorylation, indicative of increased TGFβ signaling.[60] Other genes asso-

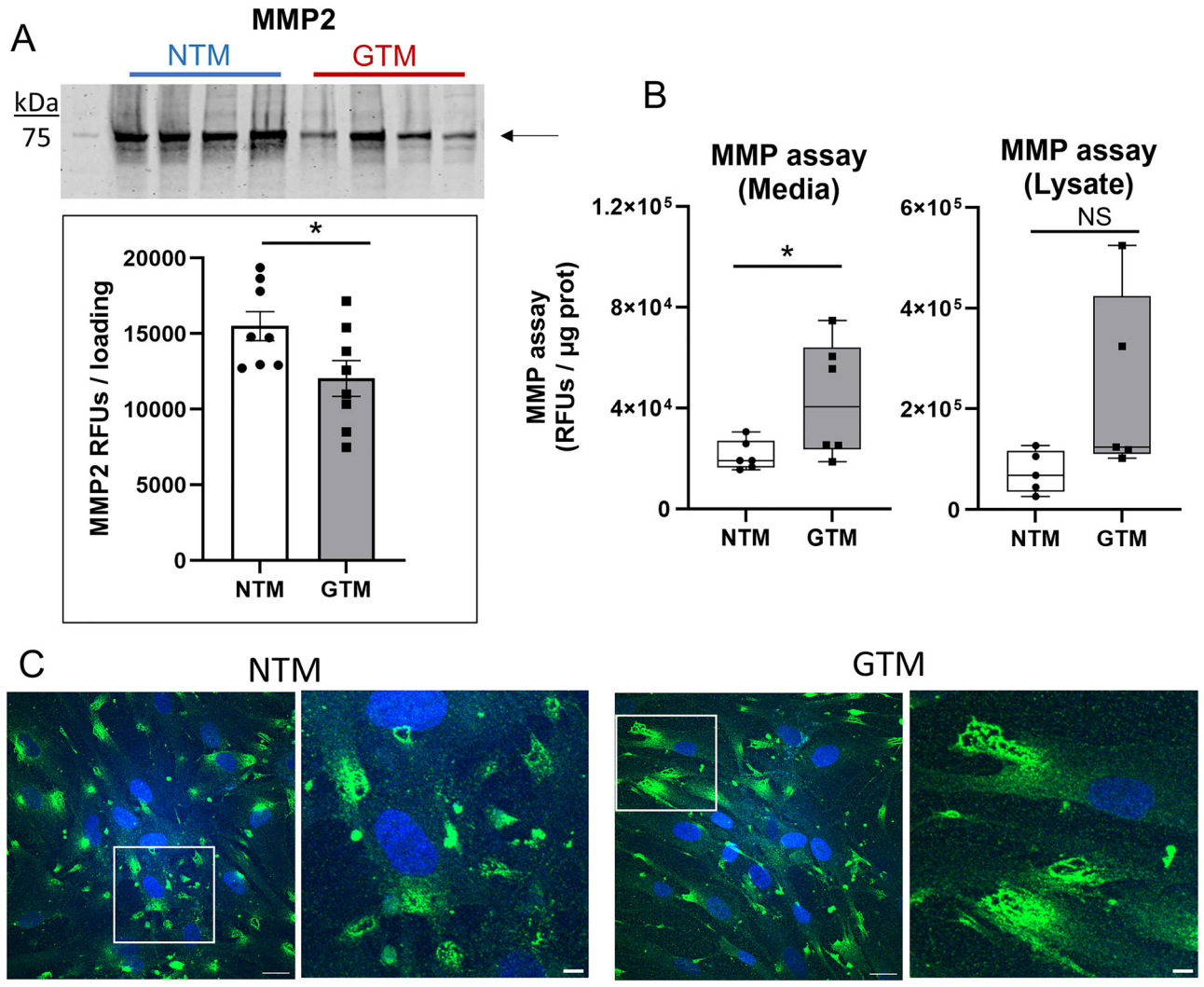

Figure 6. *MMP2* in NTM and GTM cells. (**A**) Western immunoblot and densitometry of MMP2 protein RFUs ± SEM in conditioned media shows a significant decrease in MMP2 protein levels in GTM cells. *$P < 0.05$; $n = 8$ from 4 biological replicates. (**B**) MMP activity assay shows that GTM cells had significantly increased MMP activity in the conditioned media than NTM cells. *$P = 0.047$; $n = 6$ biological replicates each. MMP activity in the GTM lysates was also increased, but this did not reach significance ($P = 0.068$). (**C**) Representative immunofluorescence images of MMP2 in NTM and GTM cells. MMP2 was localized in PILS, which were larger in GTM cells. *Scale bar* = 20 µm.

ciated with the TGFβ pathway, SMAD6, and activin A receptor type II-like 1 (*ACVRL1* or ALK1), were downregulated in GTM cells. Downregulation of SMAD6 is consistent with an EndMT phenotype because in arterial endothelial cells subject to shear stress, downregulation resulted in reduced cell-cell junctions, loss of endothelial cell barrier function, and enhanced expression of mesenchymal markers.[61] Yet, the endothelial EndMT biomarkers, VE-cadherin, eNOS, and *PECAM-1* did not produce a sufficient signal to be detected in our study. These genes are considered to be more closely associated with Schlemm's canal endothelial cells,[62] so it is perhaps not surprising that they did not produce a signal in TM cells. Thus, whereas GTM cells upregulate numerous mesenchymal markers that are consistent with an EndMT phenotype, we did not see a downregulation of endothelial biomarkers. This could reflect differences in EndMT biomarkers expressed by vascular endothelial cells and TM cells, especially considering that TM cells are not true endothelial cells.[63] EndMT is a complex and dynamic process and cell cultures are not a pure population of either endothelial or mesenchymal/myofibroblastic cells, but rather during the transition, the cell population are in various intermediary states called "partial EndMT."[64] A recent study described partial EndMT in NTM cells.[65] Compression of NTM cells seeded in hydrogels induced expression of several EndMT biomarkers (αSMA, fibronectin, and TGFβ2), indicative of partial EndMT, whereas concurrent treatment with TGFβ2 induced full mesenchymal transition, as indicated by upregulation of *TWIST1* and N-cadherin. Thus, some of our GTM cell gene expression profiles are consistent with a partial-EndMT phenotype, where cells display properties of both endothelial and mesenchymal cells,[66] and some GTM cells are likely to have undergone full mesenchymal transition. It is also likely that some NTM cell strains may be starting EndMT because these cells were derived from older individuals. This would explain why there is some variability in expression levels of some of the biomarkers in the data herein.

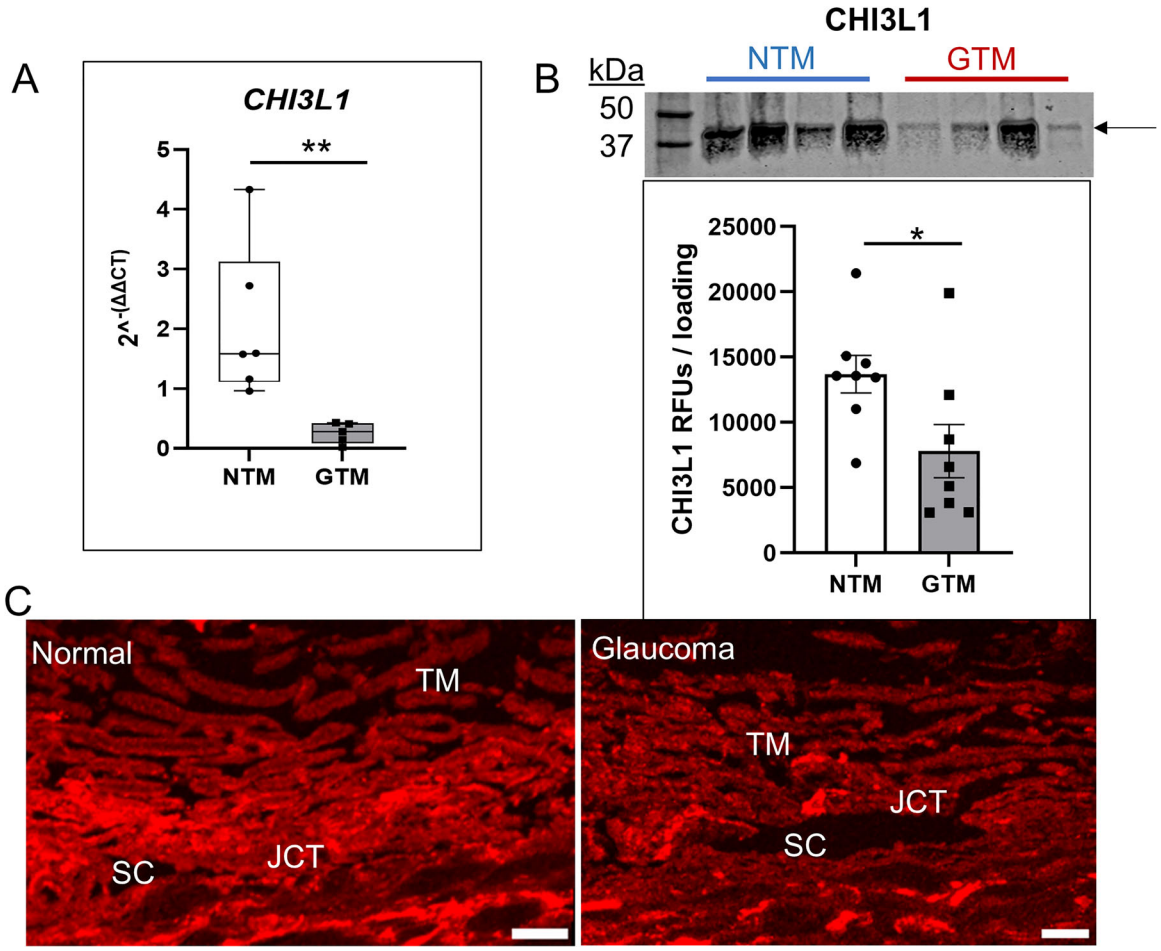

Figure 7. *CHI3L1* in NTM and GTM cells. (**A**) Quantitative RT-PCR using Taq Man primer-probes shows significant downregulation of the *CHI3L1* gene in GTM cells. NTM, $n = 6$ biological replicates; GTM, $n = 5$ biological replicates; $^{**}P < 0.01$. (**B**) Representative Western immunoblot and densitometry of CHI3L1 RFUs ± SEM in conditioned media shows a significant decrease in CHI3L1 protein levels in GTM cells. $^{*}P < 0.05$; $n = 8$ from 4 biological replicates. (**C**) CHI3L1 distribution in normal and glaucoma TM tissue. SC, Schlemm's canal; TM, trabecular meshwork. *Scale bar* = 20 µm.

Several previous studies have investigated gene expression between normal and glaucomatous TM.[24–26] However, very few of the significant DEGs identified in their studies were found in our results. This could be due to several key differences. The NanoString panel has a subset of fibrosis-related genes on it, which limits the identification of significant genes across the entire genome. In the Liton study, the cultured TM cells were from cadaver eyes that were significantly younger (42 years) than those used for the tissue (77 years). Thus, some of the DEGs identified may represent age-related changes, as we have recently described (Faralli et al., IOVS, 2024, 65, E-abstract 5165). In addition, our study cultured TM cells in the presence of ascorbate, which increases synthesis of collagens like COL6A3,[67] whereas the Liton study did not. In an analysis of POAG tissue using Illumina arrays, two genes were common to our study: N-cadherin and *VCAM1*.[26] N-cadherin was upregulated 3.33-fold in POAG tissues, consistent with the upregulation that we found in our cultured GTM cells. However, *VCAM1* was upregulated 2.41-fold in POAG tissue in their study, whereas it was significantly downregulated in GTM cells in the present study. These results suggest that some, but not all, glaucomatous changes may be maintained when GTM cells are cultured. However, glaucoma is a heterogenous disease and due to biological variation, not all patients with glaucoma will exhibit the same gene expression profiles and differences are to be expected.

Although MMP2 mRNA expression and protein levels were significantly reduced in GTM cells, MMP activity was increased. Most MMPs are regulated at the transcriptional level, with the exception of MMP2.[68] MMP2 is controlled via a unique mechanism involving a tri-molecular activation complex with MMP14 and TIMP2.[69] Thus, small changes in the levels of MMP14 and/or TIMP2 can affect MMP2 activity. However, the most logical explanation for the increased MMP activity in GTM cells is that other MMPs also contribute because this assay was not specific for MMP2.

Our study found decreased levels of CHI3L1 and COL6A3 in GTM cells. CHI3L1 plays a role in ECM remodeling and suppresses cell-cell junction genes, such as E-cadherin.[70] Thus, CHI3L1 has been implicated as playing a role in fibrosis. In the TM, CHI3L1 is highly expressed and is used as a specific biomarker of TM cells. However, in our study, CHI3L1 protein levels were variable in individual TM cell strains, with some strains showing robust levels, whereas others had little to no CHI3L1 protein. This variability was

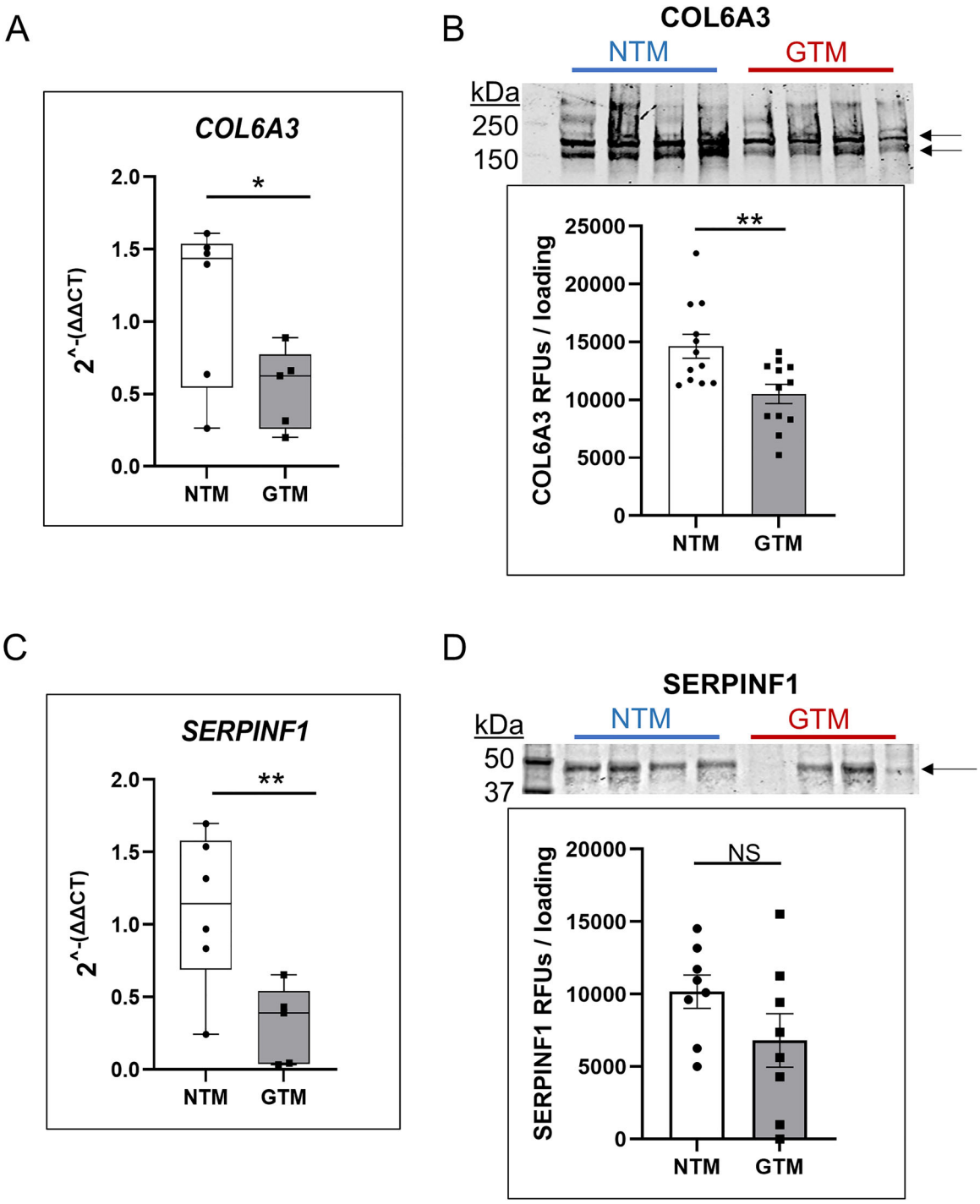

Figure 8. *COL6A3* and *SERPINF1* in NTM and GTM cells. (**A**) Quantitative RT-PCR using Taq Man primer-probes shows significant downregulation of the *COL6A3* gene in GTM cells. NTM, $n = 6$ biological replicates; GTM, $n = 5$ biological replicates; $^{*}P < 0.05$. (**B**) Representative Western immunoblot and densitometry of COL6A3 RFUs ± SEM in conditioned media shows a significant decrease in COL6A3 protein levels in GTM cells. $^{**}P < 0.01$; $n = 12$ from 5 biological replicates each of NTM and GTM. (**C**) Quantitative RT-PCR using Taq Man primer-probes shows significant downregulation of the *SERPINF1* gene in GTM cells. NTM, $n = 6$ biological replicates; GTM, $n = 5$ biological replicates; $^{**}P < 0.01$. (**D**) Representative Western immunoblot and densitometry did not detect a significant change in SERPINF1 RFUs in conditioned media from GTM cells. Not significant (NS); $n = 8$ from 4 biological replicates.

not dependent on disease status. The significant downregulation of *COL6A3* in GTM cells identified in this study corroborates our previous study, which showed that COL6A3 protein deposition into the ECM was highly reduced.[57] It is possible that genetic variation in these primary cell strains, particularly in GTM cells, may influence CHI3L1 and COL6A3 protein levels. *CHI3L1* genetic variants are associated with CHI3L1 protein levels in plasma samples in the general population,[71] whereas *COL6A3* gene variants are associated with IOP and glaucoma.[57,58] None of the GTM cells used in

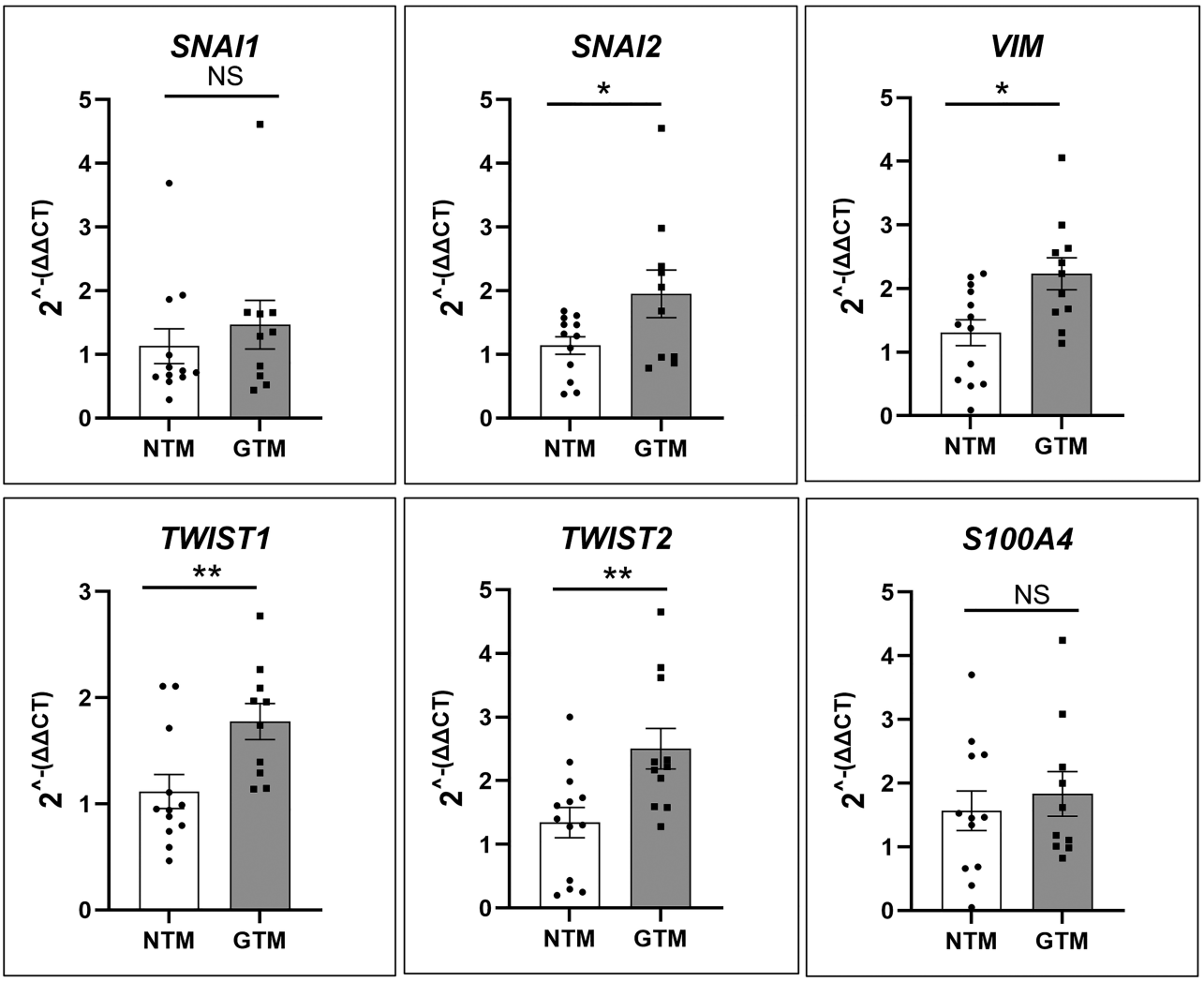

Figure 9. Classic EndMT biomarker gene expression. Quantitative RT-PCR using Taq Man primer-probes of EndMT biomarkers *SNAI1*, *SNAI2* (*SLUG*), *VIM*, *TWIST1*, *TWIST2*, and *S100A4*. NTM, $n = 9$ biological replicates; GTM, $n = 7$ biological replicates; $^{*}P < 0.05$; $^{**}P < 0.01$; NS, not significant.

this study have the rare D563G *COL6A3* variant we previously reported (data not shown),[57] but we did not sequence the entire gene so other *COL6A3* gene variants may be present. In addition, we did not sequence *CHI3L1*. However, it seems likely that genetic variation, or epigenetic regulation, may influence expression of certain genes in GTM cells.

Fibronectin is a large multi-domain extracellular molecule, which interacts with cell surface integrin molecules and plays a major role in cell adhesion. Expression of its EDA isoform is believed to play an important role in the transition into a myofibroblast and is stimulated by TGFβ signaling in TM.[51,52] When constitutively expressed, FN-EDA increases IOP in mice suggesting that it is a cause for glaucoma.[72] Our results show that FN-EDA levels were increased in GTM fibronectin fibrils, which is consistent with a prior study using GTM cells.[52] Interestingly, we also found that GTM cells have significantly decreased levels of FN-EDB compared to NTM cells. The EDB domain is a highly conserved 91 amino acid domain that is inserted between fibronectin type III repeats 7 and 8 of cellular fibronectin.[51] The function of EDB isoform is not entirely clear. A previous study linked EDB expression to increased phagocytosis.[73] Matrices containing less FN-EDB in their fibronectin fibrils may reduce the phagocytic capacity of GTM cells. Consistent with this, our group and others have shown that phagocytosis is impaired in GTM cells compared with age-matched NTM cells.[41,74] Other structural studies revealed that inclusion of EDB into fibronectin fibrils causes reorganization of the RGD loop, allowing two integrins to bind at the same time.[75] Reduced FN-EDB in GTM cells therefore suggest altered integrin binding and clustering. This is consistent with the altered pattern of active $\alpha5\beta1$ and $\alpha v\beta3$ integrin staining in GTM cells. The extensive $\alpha v\beta3$ integrin immunostaining was particularly intriguing, and the size of the focal adhesions were similar to "supermature" adhesions.[76,77] These large focal adhesions help to recruit αSMA to stress fibers, which is consistent with the upregulation of αSMA in GTM cells.

Glaucoma TM tissue is in limited supply and contains few TM cells, which limits the number and type of functional assays that can be performed using tissue. Increasing evidence shows that TM cells retain a mechanical memory.[78] The mechanomemory concept proposes that cells maintain their phenotype when they are removed from their original

biomechanical environment and placed in a new one.[79,80] For instance, fibroblasts cultured on stiff substrates mimicking fibrosis maintained their transition to a myofibroblast phenotype even when re-plated onto a soft substrate.[79] Similarly, our results as well as prior studies suggest that cultured human TM cells retained expression of numerous genes found in TM tissue.[24] Furthermore, healthy TM cells grown on hydrogels mimicking the stiffness of glaucoma TM tissue adopted a glaucoma-like phenotype[81] and had altered YAP/TAZ, molecules involved in mechanotransduction.[82–84] TM cells grown from stiff, glaucomatous tissue have thicker actin stress fibers[41] and synthesize an ECM that was molecularly different from TM cells derived from softer, non-diseased tissue.[85] Thus, the data presented in this study suggests that, in combination with tissue studies, cultured TM cells are a useful in vitro model for studying glaucoma.

In conclusion, our study using cultured TM cells identified 30 fibrotic-related genes and proteins that are differentially expressed in glaucoma. Several of these genes are consistent with glaucoma cells undergoing partial- or full-EndMT. The link connecting EndMT, fibrosis, and glaucoma is important as we consider the design of new therapeutic agents to reduce elevated IOP and treat patients with glaucoma.

Acknowledgments

The authors thank VisionGift, Portland, Oregon, and Wisconsin Lions Eye Bank for procurement of human cadaver eyes.

Supported by NIH grants EY032590 (KEK), EY019643 (KEK), and P30 EY010572 core facility grant at Casey Eye Institute, and by R01EY017006 (DMP), R01EY032905 (DMP), P30 EY016665 (DMP) at that University of Wisconsin at Madison. Additional support at the Casey Eye Institute is provided by the Malcolm M. Marquis, MD Endowed Fund for Innovation, and by unrestricted departmental funding from Research to Prevent Blindness (New York, NY).

Disclosure: **Y.-F. Yang**, None; **P. Holden**, None; **Y.Y. Sun**, None; **J.A. Faralli**, None; **D.M. Peters**, None; **K.E. Keller**, None

References

1. Acott TS, Vranka JA, Keller KE, Raghunathan V, Kelley MJ. Normal and glaucomatous outflow regulation. *Prog Retin Eye Res*. 2021;82:100897.
2. Fuchshofer R, Tamm ER. Modulation of extracellular matrix turnover in the trabecular meshwork. *Exp Eye Res*. 2009;88:683–688.
3. Keller KE, Aga M, Bradley JM, Kelley MJ, Acott TS. Extracellular matrix turnover and outflow resistance. *Exp Eye Res*. 2009;88:676–682.
4. Bradley JM, Vranka J, Colvis CM, et al. Effect of matrix metalloproteinases activity on outflow in perfused human organ culture. *Invest Ophthalmol Vis Sci*. 1998;39:2649–2658.
5. Weinreb RN, Robinson MR, Dibas M, Stamer WD. Matrix metalloproteinases and glaucoma treatment. *J Ocul Pharmacol Ther*. 2020;36:208–228.
6. Acott TS, Kelley MJ. Extracellular matrix in the trabecular meshwork. *Exp Eye Res*. 2008;86:543–561.
7. Keller KE, Peters DM. Pathogenesis of glaucoma: Extracellular matrix dysfunction in the trabecular meshwork - a review. *Clin Exp Ophthalmol*. 2022;50:163–182.
8. Rohen JW, Futa R, Lutjen-Drecoll E. The fine structure of the cribriform meshwork in normal and glaucomatous eyes as seen in tangential sections. *Invest Ophthalmol Vis Sci*. 1981;21:574–585.
9. Tektas OY, Lutjen-Drecoll E. Structural changes of the trabecular meshwork in different kinds of glaucoma. *Exp Eye Res*. 2009;88:769–775.
10. Tamm ER. The trabecular meshwork outflow pathways: structural and functional aspects. *Exp Eye Res*. 2009;88:648–655.
11. Gong H, Freddo TF, Johnson M. Age-related changes of sulfated proteoglycans in the normal human trabecular meshwork. *Exp Eye Res*. 1992;55:691–709.
12. Gong H, Tripathi RC, Tripathi BJ. Morphology of the aqueous outflow pathway. *Microsc Res Tech*. 1996;33:336–367.
13. Alvarado J, Murphy C, Polansky J, Juster R. Age-related changes in trabecular meshwork cellularity. *Invest Ophthalmol Vis Sci*. 1981;21:714–727.
14. Liton PB, Challa P, Stinnett S, Luna C, Epstein DL, Gonzalez P. Cellular senescence in the glaucomatous outflow pathway. *Exp Gerontol*. 2005;40:745–748.
15. Ahlstrom JD, Erickson CA. The neural crest epithelial-mesenchymal transition in 4D: a 'tail' of multiple non-obligatory cellular mechanisms. *Development*. 2009;136:1801–1812.
16. Acloque H, Adams MS, Fishwick K, Bronner-Fraser M, Nieto MA. Epithelial-mesenchymal transitions: the importance of changing cell state in development and disease. *J Clin Invest*. 2009;119:1438–1449.
17. Alvandi Z, Bischoff J. Endothelial-mesenchymal transition in cardiovascular disease. *Arterioscler Thromb Vasc Biol*. 2021;41:2357–2369.
18. Zeisberg EM, Tarnavski O, Zeisberg M, et al. Endothelial-to-mesenchymal transition contributes to cardiac fibrosis. *Nat Med*. 2007;13:952–961.
19. Piera-Velazquez S, Jimenez SA. Endothelial to mesenchymal transition: role in physiology and in the pathogenesis of human diseases. *Physiol Rev*. 2019;99:1281–1324.
20. Ma J, Sanchez-Duffhues G, Goumans MJ, Ten Dijke P. TGF-beta-induced endothelial to mesenchymal transition in disease and tissue engineering. *Front Cell Dev Biol*. 2020;8:260.
21. Sabbineni H, Verma A, Somanath PR. Isoform-specific effects of transforming growth factor beta on endothelial-to-mesenchymal transition. *J Cell Physiol*. 2018;233:8418–8428.
22. Tripathi RC, Li J, Chan WF, Tripathi BJ. Aqueous humor in glaucomatous eyes contains an increased level of TGF-beta 2. *Exp Eye Res*. 1994;59:723–727.
23. Yue BY. The extracellular matrix and its modulation in the trabecular meshwork. *Surv Ophthalmol*. 1996;40:379–390.
24. Liton PB, Luna C, Challa P, Epstein DL, Gonzalez P. Genome-wide expression profile of human trabecular meshwork cultured cells, nonglaucomatous and primary open angle glaucoma tissue. *Mol Vis*. 2006;12:774–790.
25. Diskin S, Kumar J, Cao Z, et al. Detection of differentially expressed glycogenes in trabecular meshwork of eyes with primary open-angle glaucoma. *Invest Ophthalmol Vis Sci*. 2006;47:1491–1499.
26. Liu Y, Allingham RR, Qin X, et al. Gene expression profile in human trabecular meshwork from patients with primary open-angle glaucoma. *Invest Ophthalmol Vis Sci*. 2013;54:6382–6389.
27. Bhattacharya SK, Annangudi SP, Salomon RG, Kuchtey RW, Peachey NS, Crabb JW. Cochlin deposits in the trabecular meshwork of the glaucomatous DBA/2J mouse. *Exp Eye Res*. 2005;80:741–744.
28. Micera A, Quaranta L, Esposito G, et al. Differential protein expression profiles in glaucomatous trabecular meshwork: an evaluation study on a small primary open angle glaucoma population. *Adv Ther*. 2016;33:252–267.

29. Lutjen-Drecoll E, Shimizu T, Rohrbach M, Rohen JW. Quantitative analysis of 'plaque material' in the inner- and outer wall of Schlemm's canal in normal– and glaucomatous eyes. *Exp Eye Res*. 1986;42:443–455.
30. Rohen JW, Lutjen-Drecoll E, Flugel C, Meyer M, Grierson I. Ultrastructure of the trabecular meshwork in untreated cases of primary open-angle glaucoma (POAG). *Exp Eye Res*. 1993;56:683–692.
31. Lutjen-Drecoll E, Rittig M, Rauterberg J, Jander R, Mollenhauer J. Immunomicroscopical study of type VI collagen in the trabecular meshwork of normal and glaucomatous eyes. *Exp Eye Res*. 1989;48:139–147.
32. Kuchtey J, Kuchtey RW. The microfibril hypothesis of glaucoma: implications for treatment of elevated intraocular pressure. *J Ocul Pharmacol Ther*. 2014;30:170–180.
33. Knepper PA, Goossens W, Palmberg PF. Glycosaminoglycan stratification of the juxtacanalicular tissue in normal and primary open-angle glaucoma. *Invest Ophthalmol Vis Sci*. 1996;37:2414–2425.
34. Flugel-Koch C, Ohlmann A, Fuchshofer R, Welge-Lussen U, Tamm ER. Thrombospondin-1 in the trabecular meshwork: localization in normal and glaucomatous eyes, and induction by TGF-beta1 and dexamethasone in vitro. *Exp Eye Res*. 2004;79:649–663.
35. Konz DD, Flugel-Koch C, Ohlmann A, Tamm ER. Myocilin in the trabecular meshwork of eyes with primary open-angle glaucoma. *Graefes Arch Clin Exp Ophthalmol*. 2009;247:1643–1649.
36. Last JA, Pan T, Ding Y, et al. Elastic modulus determination of normal and glaucomatous human trabecular meshwork. *Invest Ophthalmol Vis Sci*. 2011;52:2147–2152.
37. Overby DR, Zhou EH, Vargas-Pinto R, et al. Altered mechanobiology of Schlemm's canal endothelial cells in glaucoma. *Proc Natl Acad Sci USA*. 2014;111:13876–13881.
38. Tamm ER, Braunger BM, Fuchshofer R. Intraocular pressure and the mechanisms involved in resistance of the aqueous humor flow in the trabecular meshwork outflow pathways. *Prog Mol Biol Transl Sci*. 2015;134:301–314.
39. Qin M, Yu-Wai-Man C. Glaucoma: novel antifibrotic therapeutics for the trabecular meshwork. *Eur J Pharmacol*. 2023;954:175882.
40. Keller KE, Bhattacharya SK, Borras T, et al. Consensus recommendations for trabecular meshwork cell isolation, characterization and culture. *Exp Eye Res*. 2018;171:164–173.
41. Sun YY, Bradley JM, Keller KE. Phenotypic and functional alterations in tunneling nanotubes formed by glaucomatous trabecular meshwork cells. *Invest Ophthalmol Vis Sci*. 2019;60:4583–4595.
42. Sun YY, Yang YF, Keller KE. Myosin-X silencing in the trabecular meshwork suggests a role for tunneling nanotubes in outflow regulation. *Invest Ophthalmol Vis Sci*. 2019;60:843–851.
43. Yang YF, Sun YY, Peters DM, Keller KE. The effects of mechanical stretch on integrins and filopodial-associated proteins in normal and glaucomatous trabecular meshwork cells. *Front Cell Dev Biol*. 2022;10:886706.
44. Hah YS, Chung HJ, Sontakke SB, et al. Ascorbic acid concentrations in aqueous humor after systemic vitamin C supplementation in patients with cataract: pilot study. *BMC Ophthalmol*. 2017;17:121.
45. Clark R, Nosie A, Walker T, et al. Comparative genomic and proteomic analysis of cytoskeletal changes in dexamethasone-treated trabecular meshwork cells. *Mol Cell Proteomics*. 2013;12:194–206.
46. Yang YF, Sun YY, Acott TS, Keller KE. Effects of induction and inhibition of matrix cross-linking on remodeling of the aqueous outflow resistance by ocular trabecular meshwork cells. *Sci Rep*. 2016;6:30505.
47. Aga M, Bradley JM, Wanchu R, Yang YF, Acott TS, Keller KE. Differential effects of caveolin-1 and -2 knockdown on aqueous outflow and altered extracellular matrix turnover in caveolin-silenced trabecular meshwork cells. *Invest Ophthalmol Vis Sci*. 2014;55:5497–5509.
48. Aga M, Bradley JM, Keller KE, Kelley MJ, Acott TS. Specialized podosome- or invadopodia-like structures (PILS) for focal trabecular meshwork extracellular matrix turnover. *Invest Ophthalmol Vis Sci*. 2008;49:5353–5365.
49. Horzum U, Ozdil B, Pesen-Okvur D. Step-by-step quantitative analysis of focal adhesions. *MethodsX*. 2014;1:56–59.
50. Tamm ER, Siegner A, Baur A, Lutjen-Drecoll E. Transforming growth factor-beta 1 induces alpha-smooth muscle-actin expression in cultured human and monkey trabecular meshwork. *Exp Eye Res*. 1996;62:389–397.
51. Faralli JA, Filla MS, Peters DM. Role of fibronectin in primary open angle glaucoma. *Cells*. 2019;8:1518.
52. Medina-Ortiz WE, Belmares R, Neubauer S, Wordinger RJ, Clark AF. Cellular fibronectin expression in human trabecular meshwork and induction by transforming growth factor-beta2. *Invest Ophthalmol Vis Sci*. 2013;54:6779–6788.
53. Clark K, Pankov R, Travis MA, et al. A specific alpha5beta1-integrin conformation promotes directional integrin translocation and fibronectin matrix formation. *J Cell Sci*. 2005;118:291–300.
54. Filla MS, Meyer KK, Faralli JA, Peters DM. Overexpression and activation of $\alpha v\beta 3$ integrin differentially affects TGFβ2 signaling in human trabecular meshwork cells. *Cells*. 2021;10:1923.
55. Wecker T, Han H, Borner J, Grehn F, Schlunck G. Effects of TGF-beta2 on cadherins and beta-catenin in human trabecular meshwork cells. *Invest Ophthalmol Vis Sci*. 2013;54:6456–6462.
56. Liton PB, Liu X, Stamer WD, Challa P, Epstein DL, Gonzalez P. Specific targeting of gene expression to a subset of human trabecular meshwork cells using the chitinase 3-like 1 promoter. *Invest Ophthalmol Vis Sci*. 2005;46:183–190.
57. Wirtz MK, Sykes R, Samples J, et al. Identification of missense extracellular matrix gene variants in a large glaucoma pedigree and investigation of the N700S thrombospondin-1 variant in normal and glaucomatous trabecular meshwork cells. *Curr Eye Res*. 2022;47:79–90.
58. Choquet H, Thai KK, Yin J, et al. A large multi-ethnic genome-wide association study identifies novel genetic loci for intraocular pressure. *Nat Commun*. 2017;8:2108.
59. Ogata N, Matsuoka M, Imaizumi M, Arichi M, Matsumura M. Decrease of pigment epithelium-derived factor in aqueous humor with increasing age. *Am J Ophthalmol*. 2004;137:935–936.
60. Montecchi-Palmer M, Bermudez JY, Webber HC, Patel GC, Clark AF, Mao W. TGFbeta2 induces the formation of cross-linked actin networks (CLANs) in human trabecular meshwork cells through the Smad and non-Smad dependent pathways. *Invest Ophthalmol Vis Sci*. 2017;58:1288–1295.
61. Fu W, Huo R, Yan Z, et al. Mesenchymal behavior of the endothelium promoted by SMAD6 downregulation is associated with brain arteriovenous malformation microhemorrhage. *Stroke*. 2020;51:2197–2207.
62. Heimark RL, Kaochar S, Stamer WD. Human Schlemm's canal cells express the endothelial adherens proteins, VE-cadherin and PECAM-1. *Curr Eye Res*. 2002;25:299–308.
63. Stamer WD, Clark AF. The many faces of the trabecular meshwork cell. *Exp Eye Res*. 2017;158:112–123.
64. Sha Y, Haensel D, Gutierrez G, Du H, Dai X, Nie Q. Intermediate cell states in epithelial-to-mesenchymal transition. *Phys Biol*. 2019;16:021001.
65. Lamont HC, Wright AL, Devries K, et al. Trabecular meshwork cell differentiation in response to colla-

Investigative Ophthalmology & Visual Science

gen and TGFbeta-2 spatial interactions. *Acta Biomater*. 2024;189:217–231.
66. Fang JS, Hultgren NW, Hughes CCW. Regulation of partial and reversible endothelial-to-mesenchymal transition in angiogenesis. *Front Cell Dev Biol*. 2021;9:702021.
67. Booth BA, Uitto J. Collagen biosynthesis by human skin fibroblasts. III. The effects of ascorbic acid on procollagen production and prolyl hydroxylase activity. *Biochim Biophys Acta*. 1981;675:117–122.
68. Sternlicht MD, Werb Z. How matrix metalloproteinases regulate cell behavior. *Annu Rev Cell Dev Biol*. 2001;17:463–516.
69. Strongin AY, Collier I, Bannikov G, Marmer BL, Grant GA, Goldberg GI. Mechanism of cell surface activation of 72-kDa type IV collagenase. Isolation of the activated form of the membrane metalloprotease. *J Biol Chem*. 1995;270:5331–5338.
70. Zhao T, Su Z, Li Y, Zhang X, You Q. Chitinase-3 like-protein-1 function and its role in diseases. *Signal Transduct Target Ther*. 2020;5:201.
71. Kjaergaard AD, Johansen JS, Nordestgaard BG, Bojesen SE. Genetic variants in CHI3L1 influencing YKL-40 levels: resequencing 900 individuals and genotyping 9000 individuals from the general population. *J Med Genet*. 2013;50:831–837.
72. Roberts AL, Mavlyutov TA, Perlmutter TE, et al. Fibronectin extra domain A (FN-EDA) elevates intraocular pressure through Toll-like receptor 4 signaling. *Sci Rep*. 2020;10:9815.
73. Kraft S, Klemis V, Sens C, et al. Identification and characterization of a unique role for EDB fibronectin in phagocytosis. *J Mol Med (Berl)*. 2016;94:567–581.
74. Zhang X, Ognibene CM, Clark AF, Yorio T. Dexamethasone inhibition of trabecular meshwork cell phagocytosis and its modulation by glucocorticoid receptor beta. *Exp Eye Res*. 2007;84:275–284.
75. Schiefner A, Gebauer M, Skerra A. Extra-domain B in oncofetal fibronectin structurally promotes fibrillar head-to-tail dimerization of extracellular matrix protein. *J Biol Chem*. 2012;287:17578–17588.
76. Goffin JM, Pittet P, Csucs G, Lussi JW, Meister JJ, Hinz B. Focal adhesion size controls tension-dependent recruitment of alpha-smooth muscle actin to stress fibers. *J Cell Biol*. 2006;172:259–268.
77. Fiore VF, Wong SS, Tran C, et al. αvβ3 Integrin drives fibroblast contraction and strain stiffening of soft provisional matrix during progressive fibrosis. *JCI Insight*. 2018;3:e97597.
78. Ghosh R, Herberg S. The role of YAP/TAZ mechanosignaling in trabecular meshwork and Schlemm's canal cell dysfunction. *Vision Res*. 2024;224:108477.
79. Balestrini JL, Chaudhry S, Sarrazy V, Koehler A, Hinz B. The mechanical memory of lung myofibroblasts. *Integr Biol (Camb)*. 2012;4:410–421.
80. Cambria E, Coughlin MF, Floryan MA, Offeddu GS, Shelton SE, Kamm RD. Linking cell mechanical memory and cancer metastasis. *Nat Rev Cancer*. 2024;24:216–228.
81. Schlunck G, Han H, Wecker T, Kampik D, Meyer-ter-Vehn T, Grehn F. Substrate rigidity modulates cell matrix interactions and protein expression in human trabecular meshwork cells. *Invest Ophthalmol Vis Sci*. 2008;49:262–269.
82. Li H, Bague T, Kirschner A, et al. A tissue-engineered human trabecular meshwork hydrogel for advanced glaucoma disease modeling. *Exp Eye Res*. 2021;205:108472.
83. Li H, Raghunathan V, Stamer WD, Ganapathy PS, Herberg S. Extracellular matrix stiffness and TGFbeta2 regulate YAP/TAZ activity in human trabecular meshwork cells. *Front Cell Dev Biol*. 2022;10:844342.
84. Raghunathan VK, Morgan JT, Dreier B, et al. Role of substratum stiffness in modulating genes associated with extracellular matrix and mechanotransducers YAP and TAZ. *Invest Ophthalmol Vis Sci*. 2013;54:378–386.
85. Raghunathan V, Benoit J, Kasetti R, et al. Glaucomatous cell derived matrices differentially modulate non-glaucomatous trabecular meshwork cellular behavior. *Acta Biomater*. 2018;71:444–459.

Investigative Ophthalmology & Visual Science